Nanoscale

SUPPORTING INFORMATION

Protein-directed crystalline 2D fullerene assemblies

Mantas Liutkus,[a]‡ Alicia López-Andarias,[b]‡ Sara H. Mejías,[a] Javier López-Andarias,[b] David Gil-Carton,[c] Ferran Feixas,[d] Sílvia Osuna,[d,e] Wakana Matsuda,[f] Tsuneaki Sakurai,[f] Shu Seki,[f] Carmen Atienza,[*b] Nazario Martín[*b,g] and Aitziber L. Cortajarena[*a,h]

Received 16th August 2019,
Accepted 5th November 2019

DOI: 10.1039/c9nr07083d

rcs.li/nanoscale

Experimental

Materials

Reagents, including [60] fullerene derivatives, were purchased from Sigma-Aldrich and were used without further purification.

Protein design and production

Molecular model of tyrosine mutations was build using Pymol. E2Y, N6A and N9Y point mutations constituting the mutated residues were introduced into C1 consensus repeat through QuikChange site-directed mutagenesis. CTPR8 proteins were constructed by sequential ligation of consensus and mutated C1 sequences into pPro-EX-HTa vector.[1] Proteins were expressed in *E.coli* C41 (DE3) cells with IPTG induction at 30 °C or 37 °C overnight. Histag-IMAC purification was carried out using HisTrap™ HP columns from GE Healthcare. The hexahistidine tags were then cleaved using TEV protease and proteins were purified by size exclusion chromatography on ÄKTApure purifier with GE Fraction collector F9-R, using HiLoad™ 16/600 SuperdexTM 75 pg column and eluting with 50 mM Tris buffer, pH 8.

Protein-fullerene coupling

Ca. 1 mg of pristine **C_{60}** or C_{60}-pyrrolidine tris-acid (**C_{60}A**) was suspended in 1 ml of the test protein in 50 mM Tris, pH 8, and the suspension was subjected to probe-tip sonication for 20 min with 0.5 s on/off cycles at 0 °C, using Sartorius stedim biotech Labsonic® P sonicator. Subsequently, the mixture was centrifuged in a bench top centrifuge at 21000 *g* for 10 min and the supernatant was purified by size exclusion chromatography on ÄKTApurifier with Frac-950 fraction collector, using Superdex™ 75 10/300 GL column, eluting with 50 mM Tris buffer, pH 8, and collecting fractions of 0.5 ml.

Circular dichroism (CD) measurements

CD spectra were recorded using a Jasco J-815 CD Spectrometer in a 0.1 cm path length quartz cuvette, acquired with a band-width of 1 nm at 1 nm increments and 10 s average time.

Thermal denaturation was performed in a 0.1 cm path length quartz cuvette in MilliQ water or, in the case of **CTPR8Y_{16}-C_{60}A**, in 3, 4, 5 and 6 M urea solutions. The denaturation curves were monitored by following the CD signal at 222 nm wavelength as a function of temperature from 10 °C to 95 °C.

Transmission electron microscopy (TEM)

The samples for cryo-electron microscopy (cryo-TEM) experiments were vitrified on freshly glow-discharged (high vacuum coating system MED 020 BALTEC) holey carbon grids (Holey-carbon film on Copper 200 mesh; QUANTIFOIL R 2/2). The grids were held with ultra-thin tweezers inside the chamber of a Vitrobot Mark II (FEI Company, USA), maintained at 8 °C temperature and with relative humidity close to saturation (90% rH) to prevent drying artefacts in the blotting process. Four microliters of the sample solution were adsorbed onto the grid for 30 seconds and most of the liquid in the grid was removed by automatically blotting the grid (blot time = 3 seconds, number of blots = 1, drain time = zero and blot offset = -3 mm) with absorbent standard Vitrobot filter paper (Ø55/20mm, Grade 595, Thermo Fisher Scientific FEI) to create an "ultra-thin liquid film" (i.e., typically bellow ~100 nm film thicknesses). After the blotting, the grid was abruptly plunged into a liquid ethane bath, previously cooled with liquid nitrogen to approximately -180 °C. Vitrified grids were then removed from the plunger and stored under liquid nitrogen.

High resolution zero tilt two-dimensional (2D) images were collected on a JEM-2200FS/CR (JEOL, Ltd.) field emission gun (FEG) transmission electron microscope, operated at 200 kV at liquid nitrogen temperature, using a 626 DH cryo transfer holder (Gatan Inc.). An in-column Ω energy filter was used to record images with improved signal to noise ratio by zero-loss filtering, with the energy slit width set at 15 eV. Digital images were recorded under low-dose conditions (on the order of 20-30 electrons/Å² per exposure) with an under-focus range from 2.0 to 5.0 μm using DigitalMicrograph™ (Gatan) software with a 4K × 4K Ultrascan4000™ CCD camera (Gatan Inc.).

For electron tomography, a single-axis tilt series of ± 64° with 2° increments was recorded with under-focus values ranging from 5 to 8 μm, using a 914 high tilt liquid nitrogen cryo transfer tomography holder (Gatan Inc.). Semiautomatic data acquisition software SerialEM[2] was used for data collection. Vitrified grids contained 10 nm gold nanoparticles for image alignment. Other conditions as described above.

Computational Methods. Molecular Dynamics Simulations

The parameters for the [60]fullerene species, **C_{60}** or **C_{60}A**, for the MD simulations were generated within the ANTECHAMBER module

of AMBER 16[3] using the general AMBER force field (GAFF)[4], with partial charges set to fit the electrostatic potential generated at the HF/6-31G(d) level by the RESP model.[5] The charges were calculated according to the Merz-Singh-Kollman scheme[6, 7] using Gaussian 09.[8] MD simulations of **CTPR8** were carried out using PDB 2HYZ as a reference, removing the crystallised samarium ion. The starting structure for the MD simulations of **CTPR8Y$_{16}$** was prepared by manually introducing the abovementioned tyrosine mutations with the mutagenesis tool from PyMOL software using the **CTPR8** crystal structure (PDB 2HYZ) as starting point. In all cases, i.e. **CTPR8-C$_{60}$**, **CTPR8-C$_{60}$A**, **CTPR8Y$_{16}$-C$_{60}$** and **CTPR8Y$_{16}$-C$_{60}$A** simulations, [60]fullerenes were placed in arbitrary positions in the solvent region (more than 10 Å away from the protein surface and 20 Å far from other [60]fullerene molecules). In cases where more than one **CTPR8Y$_{16}$** unit was included in the simulation, the proteins were separated by at least 40 Å. From these coordinates, conventional MD simulations were used to allow the fullerene molecules to diffuse freely until spontaneous association with the surface of the protein, and, finally, interaction with **CTPR8** binding sites.[9] The association of **C$_{60}$A** molecules to the protein was determined by visual inspection of the MD trajectories and by measuring distances between the **C$_{60}$A** and the protein.

Each system was immersed in a pre-equilibrated truncated octahedral box of water molecules with an internal offset distance of 10 Å, using the LEAP module.[10] All systems were neutralised with explicit counterions (Na^+ or Cl^-). A two-stage geometry optimisation approach was performed. First, a short minimisation of the positions of water molecules with positional restraints on solute by a harmonic potential with a force constant of 500 kcal mol^{-1} Å^{-2} was done. The second stage was an unrestrained minimisation of all the atoms in the simulation cell. Then, the systems were gently heated in six 50 ps steps, increasing the temperature by 50 K each step (0-300 K) under constant-volume, periodic-boundary conditions and the particle-mesh Ewald approach[11] to introduce long-range electrostatic effects. For these steps, a 10 Å cut-off was applied to Lennard-Jones and electrostatic interactions. Bonds involving hydrogen were constrained with the SHAKE algorithm.[12] Harmonic restraints of 10 kcal mol^{-1} were applied to the solute, and the Langevin equilibration scheme was used to control and equalise the temperature.[13] The time step was kept at 2 fs during the heating stages, allowing potential inhomogeneities to self-adjust. Each system was then equilibrated for 2 ns with a 2 fs timestep at a constant pressure of 1 atm. Finally, conventional MD trajectories at constant volume and temperature (300 K) were collected. In total, five replicas of 800 ns MD simulations for **CTPR8** in the presence of eight **C$_{60}$**, five replicas of 800 ns MD simulations for **CTPR8** in the presence of eight **C$_{60}$A**, five replicas of 800 ns MD simulations for **CTPR8Y$_{16}$** in the presence of eight **C$_{60}$**, five replicas of 800 ns MD simulations for **CTPR8Y$_{16}$** in the presence of eight **C$_{60}$A**, five replicas of 500 ns MD simulations for **CTPR8Y$_{16}$** in the presence of twenty-four **C$_{60}$A**, and five replicas of 200 ns MD simulations for three **CTPR8Y$_{16}$** units in the presence of eight **C$_{60}$A**; gathering a total of 4 μs for each **CTPR8-C$_{60}$**, **CTPR8-C$_{60}$A**, **CTPR8Y$_{16}$-C$_{60}$** and **CTPR8Y$_{16}$-C$_{60}$A** co-assemblies, 2.5 μs for **CTPR8Y$_{16}$-24C$_{60}$A** co-assembly, and 1 μs for **3CTPR8Y$_{16}$-24C$_{60}$A** co-assembly.

Flash-Photolysis Time-Resolved Microwave Conductivity (FP-TRMC)

Nanosecond laser pulses from a Nd:YAG laser of Spectra-Physics INDI-HG (full width at half maximum ($\phi\Sigma\mu$) of 5-8 ns) was used as an excitation light source, and the third harmonic generation (THG) (355 nm) was exposed to the cast films prepared from aqueous solutions of **CTPR8-C$_{60}$**, **CTPR8-C$_{60}$A**, **CTPR8Y$_{16}$-C$_{60}$** and **CTPR8Y$_{16}$-C$_{60}$A**. The laser power density was set at 10 mW (9.1×10^{15} photons cm^{-2}). The microwave frequency and power were set at approximately 9.1 GHz and 3 mW, respectively, and the TRMC signal was evolved in a diode (rise time < 1 ns), and output signal was led into a digital oscilloscope of Tektronix TDS 3032B. All experiments were conducted at room temperature. Reflected power change ratio ($\Delta P_r/P_r$) of microwave from the cavity in FP-TRMC apparatus is in relation with the total loss ($\Delta(1/Q)$) of microwave by the photo-induced transient species in the cavity as follows[14]:

$$\frac{\Delta P_r}{P_r} = \frac{\left(\frac{1}{Q}\right)}{\left(\frac{\Delta\omega}{\omega_0}\right)^2 + \left(\frac{1}{2Q}\right)^2} \Delta\left(\frac{1}{Q}\right) \quad (2),$$

where ω_0 and $\Delta\omega$ are the resonant frequency of 9.1 GHz and its shift by the photo-induced transient species. The loss and the frequency shift of the microwave are expressed as a function of complex conductivity ($\Delta\sigma_r + i\Delta\sigma_i$) of the transient species by:

$$\Delta\left(\frac{1}{Q}\right) - i\frac{2\Delta\omega}{\omega_0} = F\left(\Delta\sigma_r + i\Delta\sigma_i\right) \quad (3),$$

where *F* is a calibration factor derived from the measurements of total loss of microwave in the cavity loaded with materials with well-known conductivity values. The value of $\Delta P_r/P_r$ is proportional to the sum of the mobilities ($\Sigma\mu$) of charged species in case of negligibly small $\Delta\omega$:

$$\Delta\sigma_r = N\phi\sum\mu = A\frac{\Delta P_R}{P_R} \quad (4),$$

where *N*, ϕ, and A are the number of absorbed photons, photo-carrier separation quantum yield, and a sensitivity factor (constant), respectively. Details in the sensitivity factor A are described elsewhere.[15]

Notes and references

1. T. Kajander, A. L. Cortajarena and L. Regan, *Methods Mol Biol*, 2006, **340**, 151-170.
2. D. N. Mastronarde, *Journal of Structural Biology*, 2005, **152**, 36-51.
3. D. A. Case, R. M. Betz, D. S. Cerutti, T. E. Cheatham, III, T. A. Darden, R. E. Duke, T. J. Giese, H. Gohlke, A. W. Goetz, N. Homeyer, S. Izadi, P. Janowski, J. Kaus, A. Kovalenko, T. S. Lee, S. LeGrand, P. Li, C. Lin, T. Luchko, R. Luo, B. Madej, D. Mermelstein, K. M. Merz, G. Monard, H. Nguyen, H. T. Nguyen,

I. Omelyan, A. Onufriev, D. R. Roe, A. Roitberg, C. Sagui, C. L. Simmerling, W. M. Botello-Smith, J. Swails, R. C. Walker, J. Wang, R. M. Wolf, X. Wu, L. Xiao and P. A. Kollman (2016), AMBER 2016, University of California, San Francisco.

4. J. Wang, R. M. Wolf, J. W. Caldwell, P. A. Kollman and D. A. Case, *J. Comp. Chem.*, 2004, **25**, 1157-1174.
5. C. I. Bayly, P. Cieplak, W. Cornell and P. A. Kollman, *J. Phys. Chem.*, 1993, **97**, 10269-10280.
6. B. H. Besler, K. M. Merz and P. A. Kollman, *J. Comp. Chem.*, 1990, **11**, 431-439.
7. U. C. Singh and P. A. Kollman, *J. Comp. Chem.*, 1984, **5**, 129-145.
8. M. J. Frisch, G. W. Trucks, H. B. Schlegel, G. E. Scuseria, M. A. Robb, J. R. Cheeseman, G. Scalmani, V. Barone, B. Mennucci, G. A. Petersson, H. Nakatsuji, M. Caricato, X. Li, H. P. Hratchian, A. F. Izmaylov, J. Bloino, G. Zheng, J. L. Sonnenberg, M. Hada, M. Ehara, K. Toyota, R. Fukuda, J. Hasegawa, M. Ishida, T. Nakajima, Y. Honda, O. Kitao, H. Nakai, T. Vreven, J. A. Montgomery Jr., J. E. Peralta, F. Ogliaro, M. Bearpark, J. J. Heyd, E. Brothers, K. N. Kudin, V. N. Staroverov, R. Kobayashi, J. Normand, K. Raghavachari, A. Rendell, J. C. Burant, S. S. Iyengar, J. Tomasi, M. Cossi, N. Rega, J. M. Millam, M. Klene, J. E. Knox, J. B. Cross, V. Bakken, C. Adamo, J. Jaramillo, R. Gomperts, R. E. Stratmann, O. Yazyev, A. J. Austin, R. Cammi, C. Pomelli, J. W. Ochterski, R. L. Martin, K. Morokuma, V. G. Zakrzewski, G. A. Voth, P. Salvador, J. J. Dannenberg, S. Dapprich, A. D. Daniels, Ö. Farkas, J. B. Foresman, J. V. Ortiz, J. Cioslowski and D. J. Fox, *Gaussian 09, Gaussian, Inc., Pittsburgh, PA*, 2009.
9. M. Biasini, S. Bienert, A. Waterhouse, K. Arnold, G. Studer, T. Schmidt, F. Kiefer, T. G. Cassarino, M. Bertoni, L. Bordoli and T. Schwede, *Nucleic Acids Res.*, 2014, **42**, W252-W258.
10. C. E. A. F. Schafmeister, W. S. Ross and V. Romanovski, LEAP, University of California, San Francisco, 1995.
11. C. Sagui and T. A. Darden, *Annu. Rev. Biophys. Biomolec. Struct.*, 1999, **28**, 155-179.
12. J.-P. Ryckaert, G. Ciccotti and H. J. C. Berendsen, *J. Comp. Phys.*, 1977, **23**, 327-341.
13. X. Wu and B. R. Brooks, *Chem. Phys. Lett.*, 2003, **381**, 512-518.
14. J. C. Slater, *Rev. Mod. Phys.*, 1946, **18**, 441-512.
15. A. Saeki, S. Seki, T. Sunagawa, K. Ushida and S. Tagawa, *Philos. Mag.*, 2006, **86**, 1261-1276.

Supporting images

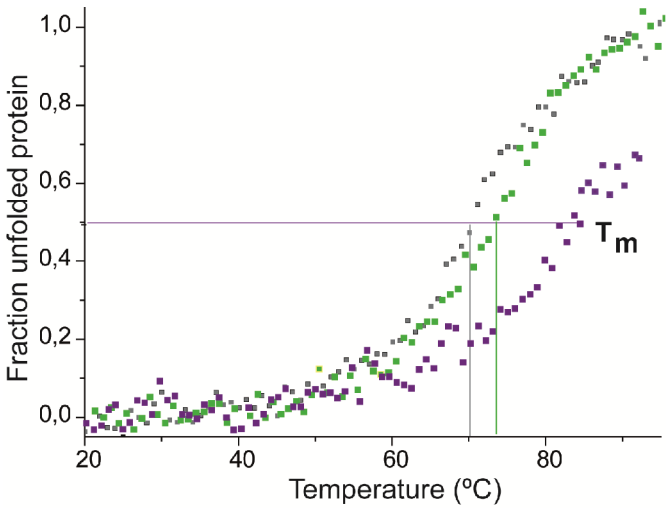

Fig. S1. CD characterisation of **CTPR8Y$_{16}$** and fullerene assemblies. Thermal denaturation profiles of **CTPR8Y$_{16}$** (gray), **CTPR8Y$_{16}$-C$_{60}$** (green) and **CTPR8Y$_{16}$-C$_{60}$A** (purple) co-assemblies, monitored by CD at 222 nm.

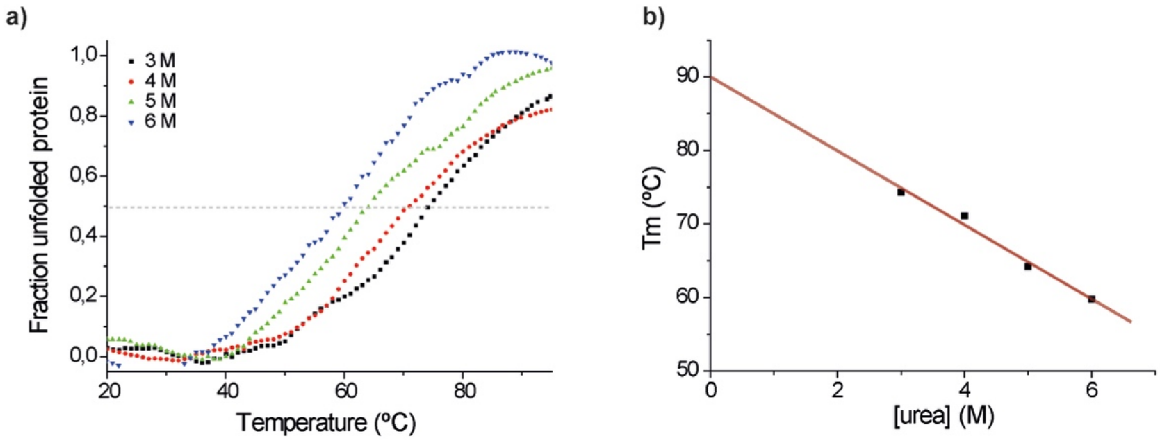

Fig. S2. Thermal stability analysis of **CTPR8Y$_{16}$-C$_{60}$A**. (a) Thermal denaturation curves in the presence of varying concentrations of urea, monitored by CD at 222 nm. (b) Relationship of T_m with the concentration of urea from part (a), allowing to extrapolate the T_m without urea.

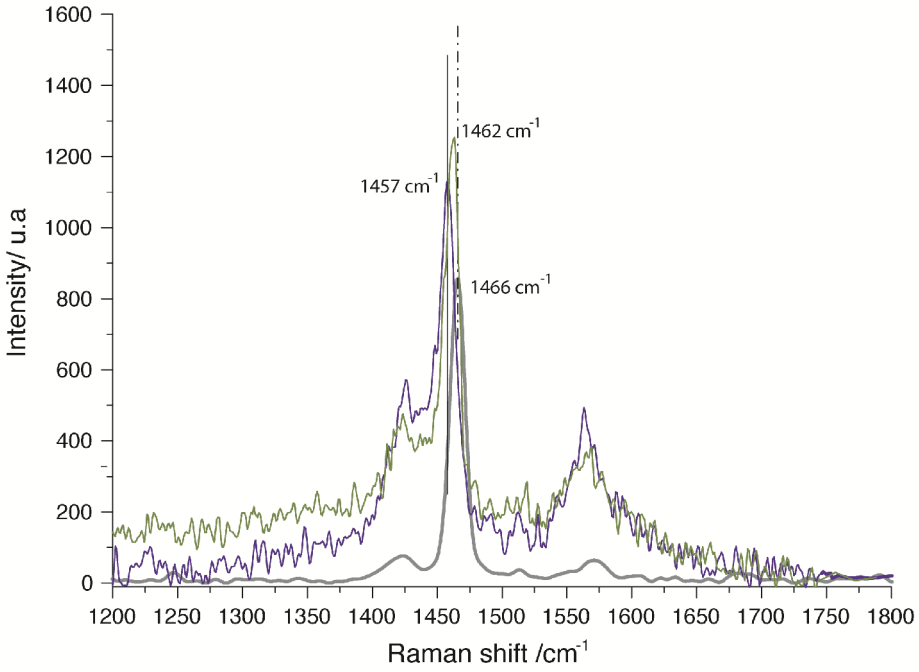

Fig. S3. Raman spectra of C_{60} (gray), **C_{60}A** (green) and **CTPR8Y$_{16}$-C_{60}A** co-assembly (purple), excited at 532 nm.

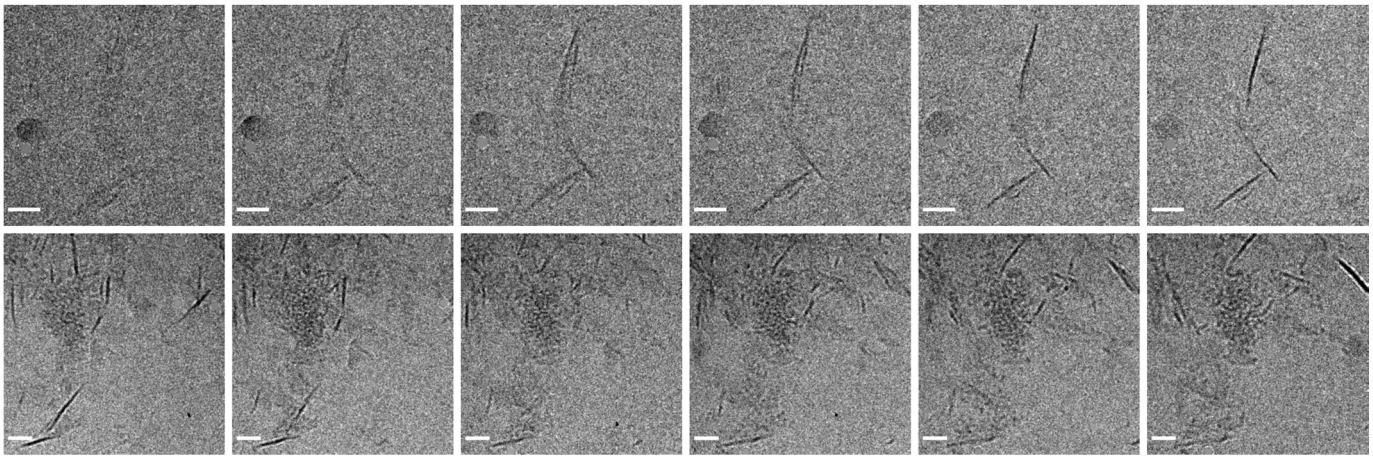

Fig. S4. Two additional series of cryo-electron micrographs of **CTPR8Y$_{16}$-C_{60}A** hybrid material at different degrees of sample tilt, showing the assemblies from different perspectives. The scale bar is 20 nm in all cases.

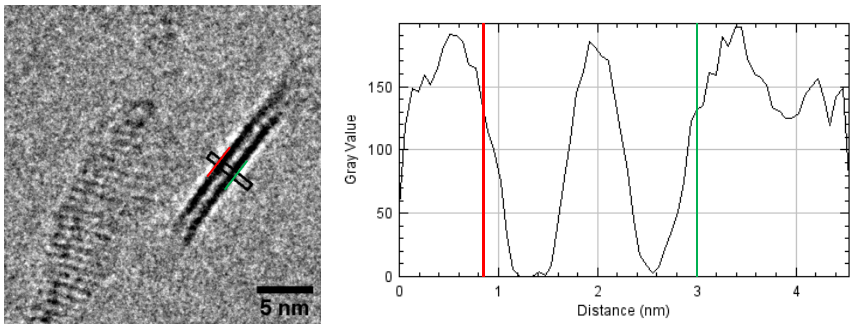

Fig. S5. Plot profile of **CTPR8Y$_{16}$-C_{60}A** assembly cryo-TEM image, showing gray values of the section indicated by black box. The entire protein-fullerene hybrid assembly, confined between the red and green marks, has the thickness of *ca*. 2 nm, consistent with the size of the protein chain. The high-contrasting (low gray value) bands defining the edges of the assembly have a rough thickness of 0.7 nm, matching the dimensions of the fullerene frame.

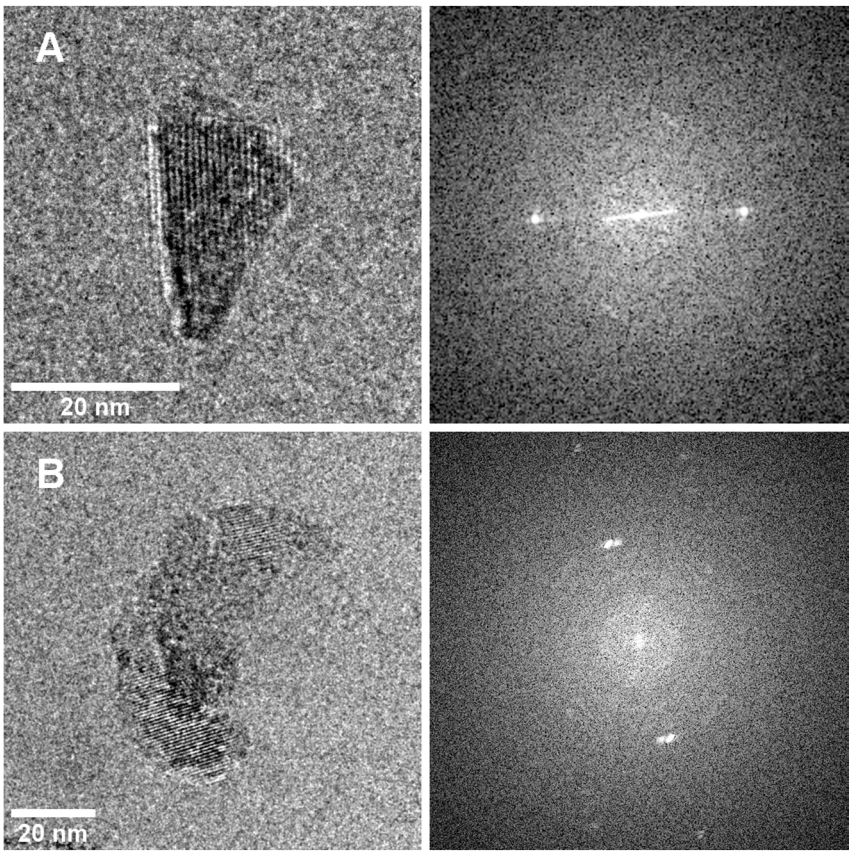

Fig. S6. Cryo-electron micrographs of (a) **CTPR8Y$_{16}$-C$_{60}$** and (b) **CTPR8-C$_{60}$** hybrid materials (left) and the corresponding FFT images (right), showing the diffraction patterns of the hybrid materials.

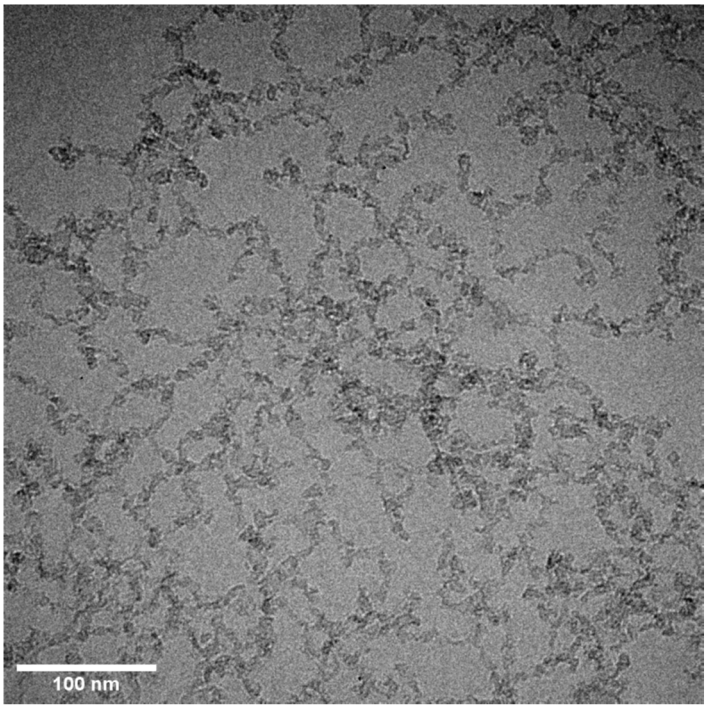

Fig. S7. Cryo-electron micrograph of fullerene-pyrrolidine tris-acid **C$_{60}$A**.

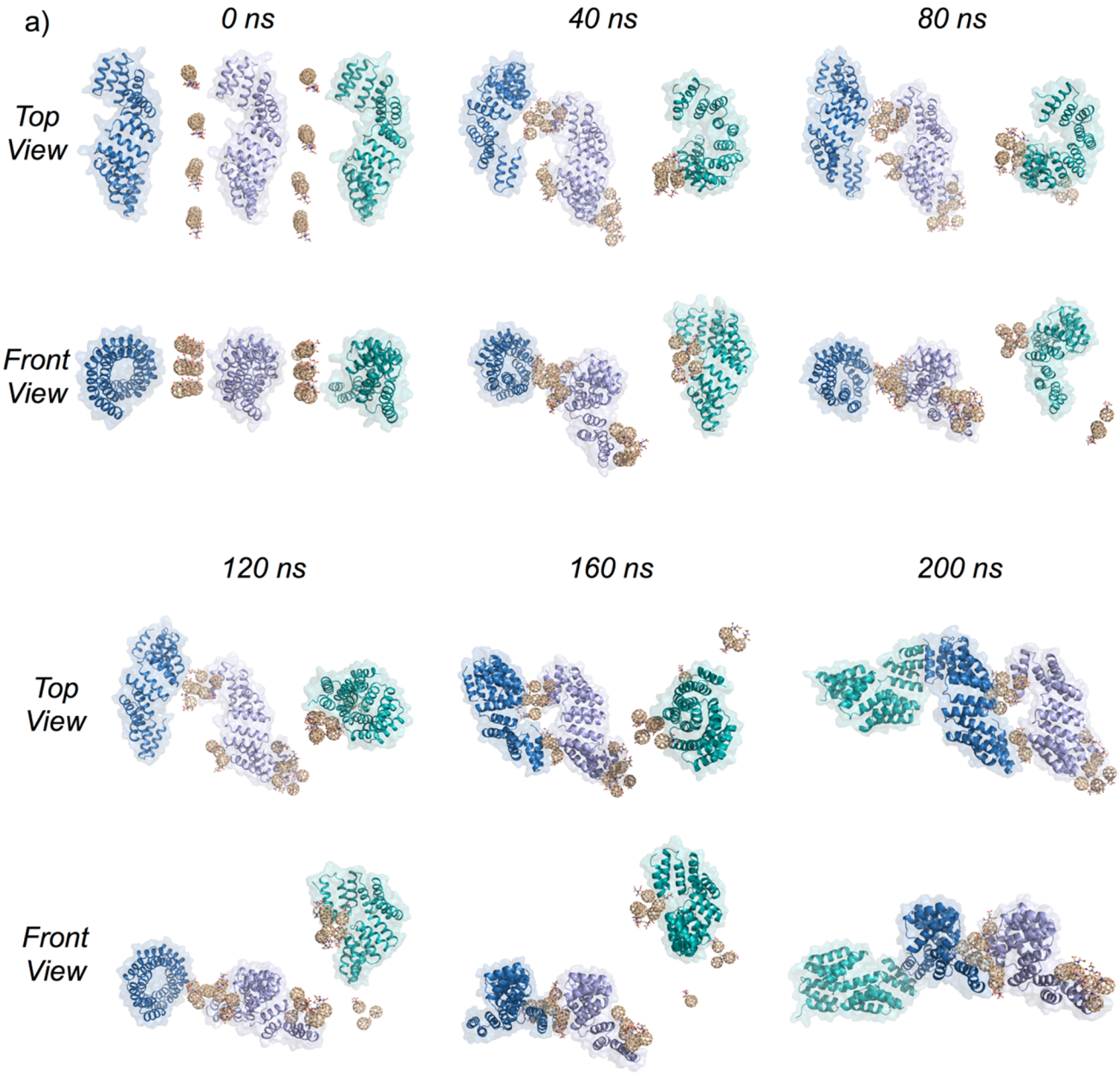
a)
0 ns
40 ns
80 ns
Top View
Front View
120 ns
160 ns
200 ns
Top View
Front View
b)
c)
Dihedral Angle
3CTPR8Y16-24C60A
Dihedral Angle
180
120
60
0
−60
−120
−180
0
50
100
150
200
Simulation time MD (ns)

Fig. S8. (previous page) MD simulation of the assembly of **CTPR8Y$_{16}$-C$_{60}$A**. (a). Top and front views of representative snapshots extracted every 40 ns from the 200 ns MD simulations of **3CTPR8Y$_{16}$-24C$_{60}$A** co-assemblies. Clusters of **C$_{60}$A** trigger the aggregation of two **CTPR8Y$_{16}$** units (events occurring at 40 ns and 160 ns). **CTPR8Y$_{16}$-C$_{60}$A** shows tendency towards alignment in a 2D plane once aggregation is produced. Note: the simulation is carried out in a solvent box considering periodic conditions, allowing the molecules to leave the box on one side and reappear on the opposite side. (b) Dihedral angle for capturing 2D packing of **CTPR8Y$_{16}$** units. To define the dihedral angle, each **CTPR8Y$_{16}$** unit is split into two parts, one that comprises the first four CTPR repeats and another that contains the last four CTPR repeats. Then, the centre of mass of each CTPR4 unit is computed, providing two centres of mass for each **CTPR8Y$_{16}$** unit. The dihedral angle illustrative of the 2D packing is then defined between the four centres of mass of two **CTPR8Y$_{16}$** units. Dihedral angles close to zero degrees indicate a two-dimensional arrangement of the two **CTPR8Y$_{16}$** units while dihedral angles that significantly deviate from zero degrees indicate a three-dimensional arrangement. (c) Plot of the dihedral angle (in degrees) along the five replicas of 200 ns MD simulations. In two out of five replicas of 200 ns, the aggregation of **CTPR8Y$_{16}$** units induced by **C$_{60}$A** is observed and in both cases the dihedral angle remains in the [-25°,25°] range upon aggregation (light blue and pink lines). In the other three replicas, full aggregation is not observed in 200 ns of MD, thus, the dihedral angle deviates from zero and is not stable along the whole MD trajectory.

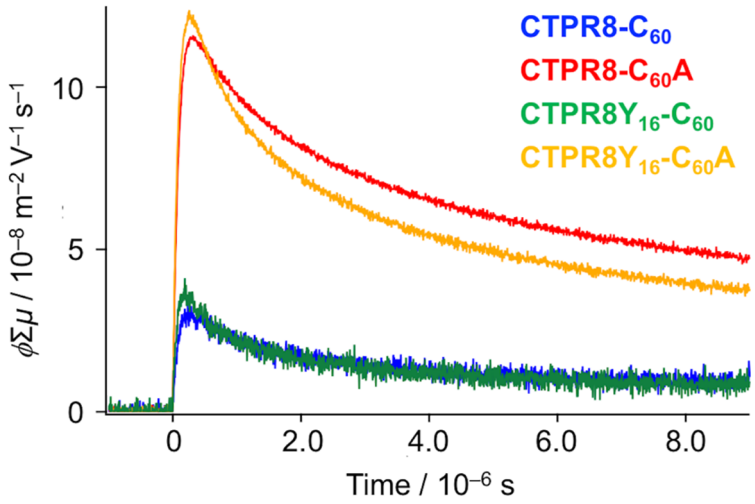

Fig. S9. Conductivity transients of dropcast films of **CTPR8-C$_{60}$** (blue), **CTPR8-C$_{60}$A** (red), **CTPR8Y$_{16}$-C$_{60}$** (green) and **CTPR8Y$_{16}$-C$_{60}$A** (yellow) co-assemblies upon photoexcitation with 355 nm pulses at photon densities of 9.1 × 10^{15} cm^{-2}, first 10 μs.